

VeTraSS: Vehicle Trajectory Similarity Search Through Graph Modeling and Representation Learning

Ming Cheng¹, Bowen Zhang², Ziyu Wang³, Ziyi Zhou¹, Weiqi Feng⁴, Yi Lyu⁵, Xingjian Diao¹

¹Dartmouth College ²Shanghai Jiao Tong University ³University of California, Irvine

⁴Harvard University ⁵Independent Researcher

{ming.cheng.gr, ziyi.zhou.gr, xingjian.diao.gr}@dartmouth.edu

zyljoy3091498@sjtu.edu.cn ziyuw31@uci.edu

wfeng@g.harvard.edu isabellalyu1130@gmail.com

Abstract

Trajectory similarity search plays an essential role in autonomous driving, as it enables vehicles to analyze the information and characteristics of different trajectories to make informed decisions and navigate safely in dynamic environments. Existing work on the trajectory similarity search task primarily utilizes sequence-processing algorithms or Recurrent Neural Networks (RNNs), which suffer from the inevitable issues of complicated architecture and heavy training costs. Considering the intricate connections between trajectories, using Graph Neural Networks (GNNs) for data modeling is feasible. However, most methods directly use existing mathematical graph structures as the input instead of constructing specific graphs from certain vehicle trajectory data. This ignores such data's unique and dynamic characteristics. To bridge such a research gap, we propose VeTraSS – an end-to-end pipeline for **Vehicle Trajectory Similarity Search**. Specifically, VeTraSS models the original trajectory data into multi-scale graphs, and generates comprehensive embeddings through a novel multi-layer attention-based GNN. The learned embeddings can be used for searching similar vehicle trajectories. Extensive experiments on the Porto and Geolife datasets demonstrate the effectiveness of VeTraSS, where our model outperforms existing work and reaches the state-of-the-art. This demonstrates the potential of VeTraSS for trajectory analysis and safe navigation in self-driving vehicles in the real world.

1. Introduction

The advancement of autonomous driving technologies has fundamentally changed transportation, leveraging cloud computing [43, 45, 46] and Location-Based Services (LBS) [14, 16, 31] to interpret the complex patterns of vehicular

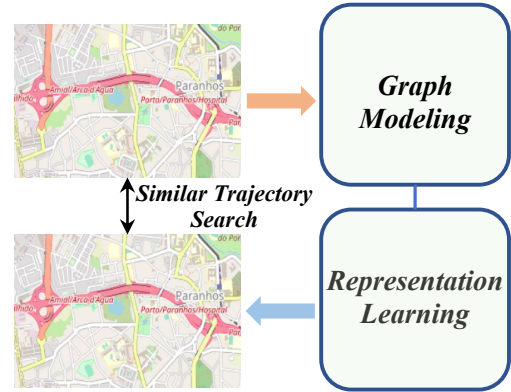


Figure 1. **Trajectory similarity search pipeline.** VeTraSS constructs the graph from the original vehicle trajectory data, followed by graph representation learning and embedding generation. The embedding is used for accurately searching alternative trajectories.

movements and human activities. This shift requires analyzing vast spatio-temporal data for improved traffic safety [41] and management [26], despite challenges from its volume and diversity. Data analysis innovations are crucial for integrating autonomous vehicles smoothly into our lives. This data offers significant potential for intelligent decision-making in health monitoring [7, 37, 38, 50] and mobile computing [1, 18], enhancing efficiency and safety in our interconnected world.

Traditionally, dimensionality reduction algorithms have served to distill the complexity of trajectory data into lower-dimensional spaces, aiding in the analysis of vehicle trajectories for autonomous driving [4, 17, 39]. These methods, while providing a foundation for understanding vehicular patterns, encounter limitations, including slow inference speeds and challenges in accurately representing the intricate details of diverse and novel real-world scenarios [2, 4, 30].

In autonomous driving, accurately predicting vehicular

movement via trajectory analysis is crucial, requiring sophisticated models to manage the complexity of vehicle trajectories. Recent shifts towards neural network-based approaches, especially those leveraging sequence processing capabilities like LSTM and RNN, have marked significant progress in spatio-temporal representation learning [15, 19, 42, 44, 47]. Yet, these models frequently entail extensive data pre-processing and bear the brunt of complex, resource-intensive training processes.

Graph Neural Networks (GNNs) [24, 29, 35, 40] have shown promise in spatio-temporal data analysis with their graph-based modeling. However, their application in autonomous driving, especially for vehicle trajectory analysis, remains underexplored. The common use of generic graph structures instead of creating specific graphs from vehicle trajectory data fails to capture its unique dynamics [12, 28, 33]. This gap prompts our research question: *How can we design an end-to-end pipeline that creates tailored graph structures from vehicle trajectory data, precisely capturing autonomous driving dynamics to improve the accuracy and relevance of trajectory similarity search?*

To bridge this research gap, we present VeTraSS, an innovative end-to-end pipeline for vehicle trajectory similarity search, as shown in Figure 1. VeTraSS models vehicle trajectories using multi-scale graphs and employs a multi-layer attention-based GNN to produce detailed embeddings to improve the search for similar trajectories, aiding autonomous vehicles in making safe, informed decisions.

In summary, our contribution is threefold:

- **End-to-end pipeline for vehicle trajectory analysis.** To the best of our knowledge, VeTraSS is the *first* pipeline tailored specifically for the autonomous driving sector, handling the entire process from graph construction of vehicle trajectories to the generation of their representations.
- **State-of-the-art performance.** Our rigorous experiments on the Porto [25] and Geolife [48] datasets, both integral to autonomous driving research, validates VeTraSS’s capability. It outperforms existing methodologies in accuracy and sets a new benchmark in vehicle trajectory similarity search.
- **Time-efficiency for representation learning.** Different from LSTM/RNN-based models, VeTraSS leverages an attention mechanism for multi-scale embedding generation. Experimental results confirm that this design excels in real-time autonomous driving applications, where quick decision-making is essential.

2. Related Work

2.1. Non-Learning-Based Methods

In autonomous driving, traditional dimensionality reduction methods like PCA [39], SVD [4], and MDS [6] were ini-

tially used for learning representations of vehicle trajectory data. These techniques aimed to reduce the complexity of spatio-temporal data by mapping it to a lower-dimensional space, making it easier to analyze and interpret. PCA works by maximizing the variance of projected sample data on a hyperplane, enhancing data representation. SVD creates a low-dimensional space through matrix decomposition, and MDS focuses on maintaining sample distances after reduction.

Despite the mathematical rigor and the theoretical promise of these techniques, they exhibit certain limitations when applied to the dynamic and varied datasets typical of autonomous driving scenarios. Specifically, they tend to suffer from slow inference speeds and a lack of flexibility in handling the diverse and unpredictable nature of real-world driving data [13, 21]. This gap between theoretical effectiveness and practical applicability has prompted the exploration of more advanced methods capable of addressing the unique challenges posed by autonomous driving data.

2.2. Sequence-Processing-Based Methods

To overcome the limitations of non-learning methods, deep learning models employing sequence processing strategies have been proposed. Sukhbaatar et al. [32] introduced an RNN structure for capturing long-term dependencies, which Chandar et al. [5] extended to a hierarchical architecture. Moreover, approaches like SRN [27] and NEUTRAJ [42] use a combination of memory networks (LSTM + RNN) for trajectory analysis, with [49] integrating Residual-LSTM for enhanced representation learning. Despite their ability to capture time-dependent features, the complexity of recurrent architectures demands significant training resources, limiting their practical application in autonomous driving.

2.3. GNN-Based Methods

Addressing the shortcomings of previous models, GNN-based approaches have emerged for graph representation learning. GGS-NN [20] employs gated recurrent units in a GNN framework, while node2vec [12] innovates in defining node neighborhoods and random walk procedures for feature representation. Liu et al. [23] introduced an unsupervised model that distinguishes between homophilic and heterophilic edges. However, these GNN models, designed for general graph-structured data, often overlook the specific requirements of spatio-temporal data in autonomous driving, such as capturing temporal dynamics and movements.

Building on this foundation, we introduce VeTraSS, a novel end-to-end pipeline that unifies spatio-temporal-specific graph construction with comprehensive representation learning, targeting the intricate dynamics of vehicle trajectories in autonomous driving environments.

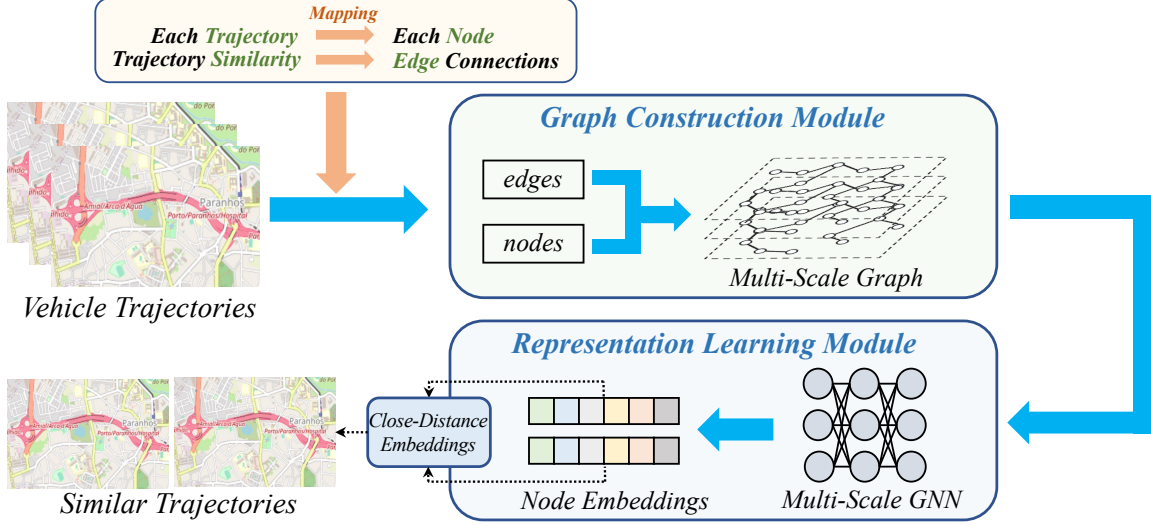


Figure 2. **Overview of the VeTraSS pipeline. Graph construction and embedding generation:** The original high-dimensional trajectories are mapped into low-dimensional space for graph construction, where each node corresponds to each trajectory while edge connections represent trajectory similarity degrees. The multi-scale graph is input into a multi-scale GNN to generate accurate node embeddings. **Trajectory similarity search:** Given a query trajectory, VeTraSS generates the corresponding embedding vector and also finds the closest embedding vector to it. The closest embedding represents the most similar trajectory.

3. Method

Considering the impossibility of directly conducting the similarity search task from the original dataset, the mathematical abstraction that maps from a high-dimensional space (trajectory dataset) into a low-dimensional one (node embedding in graphs) is necessary. After constructing the graph, a novel GNN model is designed to learn graph representations and generate node embeddings. The low-dimensional embedding vector corresponds to each high-dimensional trajectory.

The overview of the VeTraSS pipeline is shown in Figure 2. VeTraSS mainly consists of two parts, with the first one constructing the multi-scale graph from the original dataset, and the second one focusing on designing a novel attention-based GNN for precise representation learning.

3.1. Graph Construction Module

3.1.1 Similarity Matrix Generation

Assume the original vehicle trajectory dataset as $\mathcal{T} = \{T_1, T_2, \dots, T_n\}$ where T_i indicates each trajectory containing l data points:

$$T_i = \{(P_1, t_1), (P_2, t_2), \dots, (P_l, t_l)\} \quad (1)$$

Here, $P_k \in \mathcal{R}^2$ is the spatial position point corresponding to the sampling time t_k , which generally contains information on longitude and latitude. The relative magnitude of the distance between samples is used to model the similarity of

two trajectories. We define the normalized distance d_{ij} between each sample under certain distance function $dist(\cdot, \cdot)$ as:

$$d_{ij} = 1 - \frac{e^{-dist(T_i, T_j)}}{\sum_{k=1}^n e^{-dist(T_i, T_k)}} \quad (2)$$

where $dist(\cdot, \cdot)$ is Fréchet distance [11] / Hausdorff distance [3]. The distance matrix $M = (d_{ij})_{n \times n}$ is therefore constructed for the multi-layer similarity graph generation afterward.

3.1.2 Multi-Scale Graph Construction

To allow graph neural networks (GNNs) to process and model the original dataset properly, each trajectory in the dataset is mapped as a node in the graph, and the edges indicate the connection weights between two nodes, as inspired by [42]. Assume the multi-scale undirected weighted graph \mathcal{G} has m layers in total, it can be expressed as:

$$\mathcal{G} = \{G_1(V, E_1, A_1), G_2(V, E_2, A_2), \dots, G_m(V, E_m, A_m)\} \quad (3)$$

where $G_k(V, E_k, A_k)$ represents the k^{th} layer of the graph, and V is the set of nodes corresponding to the trajectories in the dataset. E_k and $A_k = (a_{k,i,j})_{n \times n}$ indicates the edges and the adjacent matrix of the k^{th} layer graph, respectively.

Since each node represents each trajectory, the node connection situations are determined by the similarity distance of trajectories (Equation 2). Specifically, since too close or distant nodes cannot establish a connection, a threshold

value c_i (both upper and lower bounds) is involved in determining whether there is a connection between node v_i and v_j in each layer of the graph. Formally, $a_{k,i,j}$, as the adjacent item between node v_i and v_j in layer k , can be defined as:

$$a_{k,i,j} = \begin{cases} 1 - d_{ij} & \text{if } c_{k-1} \leq d_{ij} \leq c_k \\ 0 & \text{otherwise} \end{cases} \quad (4)$$

Therefore, if $a_{k,i,j} > 0$, we can assume v_i and v_j form a connection in layer k , and consequently, trajectory T_i and T_j have a degree of similarity in that layer.

3.1.3 Threshold Determination

The threshold value mentioned previously needs to be determined properly. Since the distance situation satisfies the trigonometric inequality, which means for arbitrary trajectory T_r, T_p, T_q in the data \mathcal{T} , we must have:

$$d_{rp} + d_{rq} \geq d_{pq} \quad (5)$$

Without loss of generality, if assuming nodes (v_p, v_r) and (v_q, v_r) are neighbor nodes, (v_p, v_q) must not be. Therefore, following Equation 4, we have:

$$\begin{cases} c_{k-1} \leq d_{rp} < c_k \\ c_{k-1} \leq d_{rq} < c_k \\ d_{pq} \geq c_k \end{cases} \quad (6)$$

Moreover, if we need to build the connection between (v_p, v_q) in $k + 1$ layer to let the graph represent the node connection, we have:

$$c_k \leq d_{pq} < 2c_k \quad (7)$$

Therefore, if we choose the threshold value as:

$$c_k = 2c_{k-1} \quad (8)$$

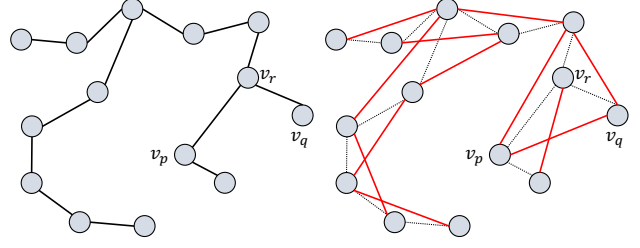
we can guarantee that (v_p, v_q) in $k + 1$ layer will form a connection, showing the comprehensive graph representation of the original data.

Following the steps above, the connection situation between each node in each layer can be determined, and therefore, the overall graph with m layers is constructed.

The qualitative example of the algorithm is shown in Figure 3, where red edges indicate the newly established connection formed in the $k + 1$ layer between nodes with a distance of 2 in layer k .

3.2. Representation Learning Module

Through Section 3.1, the graph with multi-scale is constructed, which can be further input into GNN for embedding representation learning.



(a) Graph construction in k^{th} layer (b) Graph construction in $k + 1^{th}$ layer

Figure 3. **Multi-scale graph construction.** Edge between node v_r and v_p shows the similarity between trajectory T_r and T_p . The nodes that are not connected in the k^{th} layer (with a distance of 2) will form a connection in the $k + 1^{th}$ layer, replacing the original edges.

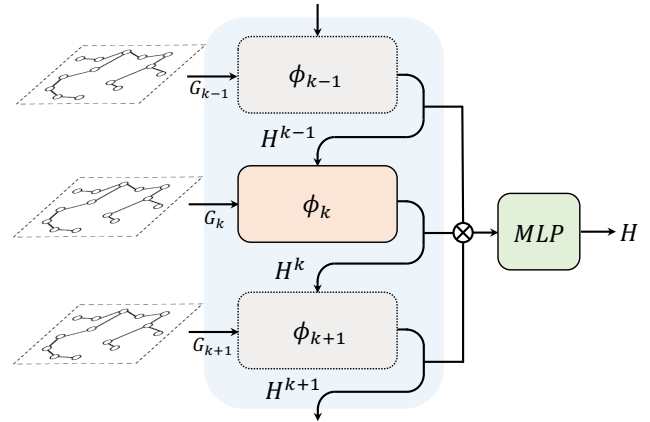


Figure 4. **Graph representation learning module.** The figure illustrates the k^{th} layer of the model, where the inputs are the graph of layer $k - 1$ (G_{k-1}) and the embedding of layer $k - 1$ (H^{k-1}), and outputs the embedding of the k^{th} layer (H^k). The final output of the model is the concatenation of each layer's output followed by an MLP module.

The architecture design is shown in Figure 4, representing an m -layer multi-scale GNN (ϕ). Since the entire model is designed in a sequential connected pattern, the module (ϕ_k) in layer k takes the k^{th} layer graph (G_k) and the $k - 1^{th}$ layer embedding representation (H^{k-1}) as the input to generate the k^{th} layer one. Specifically,

$$H^{k-1} = (h_1^{k-1}, h_2^{k-1}, \dots, h_n^{k-1}) \quad (9)$$

where $h_i^{k-1} \in \mathcal{R}^{1 \times D_{k-1}}$ represents the embedding vector of node v_i in layer $k - 1$, and D_{k-1} is the dimension of the vector.

3.2.1 Attention Mechanism

Inspired by existing attention-based architectures [8–10, 34], an attention mechanism is employed for each layer of

ϕ to measure the influence degree between the nodes. Formally, the attention coefficient between node i and j in layer k can be expressed as below:

$$w_{k,i,j} = \text{attn}(W_k h_i^{k-1}, W_k h_j^{k-1}) \quad (10)$$

where W_k represents a trainable parameter.

To avoid the paradigm expansion of the hidden state vectors which leads to the gradient explosion during training, the attention coefficient is further normalized as below:

$$\alpha_{k,i,j} = \frac{e^{w_{k,i,j}}}{\sum_{v_p \in \mathcal{N}_k(v_i)} e^{w_{k,i,p}}} \quad (11)$$

where $\mathcal{N}_k(v_i)$ indicates the neighbor node of v_i in layer k .

3.2.2 Embedding Representation Generation

The embedding representation of each node v_i , denoted as $h_i^k \in \mathcal{R}^{1 \times D_k}$ (D_k is the dimension), can be expressed through an activation function $\sigma(\cdot)$ and the normalized attention coefficient in Equation 11:

$$h_i^k = \sigma\left(\sum_{v_j \in \mathcal{N}_k(v_i)} \alpha_{k,i,j} W_k h_j^{k-1}\right) \quad (12)$$

Afterward, as expressed in Equation 9, the final output of the model in layer k is the collection of all n nodes:

$$H^k = (h_1^k, h_2^k, \dots, h_n^k) \quad (13)$$

where h_i^k indicates the embedding of node i (corresponds to trajectory T_i) in layer k .

3.2.3 Model Output

Through all m layers, the final output of the model ϕ is the concatenation of all k layers:

$$H = \text{MLP}(\text{Con}(H^1, H^2, \dots, H^k)) \quad (14)$$

where Con represents the concatenation operation and $H = (h_1, h_2, \dots, h_n)$ indicates a set of n embeddings generated by the model, and each embedding corresponds to a trajectory in the dataset.

Therefore, the original high-dimensional trajectory dataset ($T_i \in \mathcal{T}$) can be mathematically expressed as a low-dimensional embedding vector ($h_i \in H$), which can be used for efficient trajectory similarity search. Detailed procedures of trajectory similarity search are introduced in Section 4.3.

We employ cosine similarity distance as the loss function L for model training, where the loss is constructed between the generated embeddings $H \in \mathcal{R}^{N \times D}$ (N, D represent the number of trajectories and embedding dimensions, respectively) and the ground truth similarity distances $M \in \mathcal{R}^{N \times N}$ (Section 3.1.1):

$$L = \text{Cosine}(HH^T, M) \quad (15)$$

to instruct the model to generate accurate embeddings that are close to the actual similarity matrix.

4. Experiments

4.1. Dataset

We conduct extensive experiments on two widely used large-scale datasets collected from the real world, Porto [25] and Geolife [48], to thoroughly evaluate VeTraSS's performance. The Porto dataset captures over 1.7 million taxi trajectories located in the Porto area in Portugal. Specifically, it contains 1,704,759 trajectory counts, with an average of 60 data points per trajectory. The collected data are in the longitude of $(-8.735152, -8.156309)$ and the latitude of $(40.953673, 41.307945)$. Meanwhile, the Geolife dataset by Zheng *et al.* [48] presents a comprehensive collection of GPS trajectories that contains the movements of 182 individuals over five years. Specifically, it comprises over 24,876 trajectories, covering a distance exceeding 1.2 million kilometers and totaling more than 48,000 hours in duration. Geographically, the data encompasses multiple cities in China, spanning longitudes from 115.9 to 117.1 and latitudes from 39.6 to 40.7.

As publicly available real-world trajectory datasets, Porto and Geolife well reflect the complexity and variability of real-world traffic trajectories, making it an ideal dataset to be used for model performance evaluation.

4.2. Implementation Details

We preprocess the dataset by removing the trajectories having less than 50 data points, and divide the dataset into $50\text{m} \times 50\text{m}$ grids, following [42]. The embedding dimension in the model's middle layer is set as 256, while the final output embedding dimension is 128. The activation function chosen for embedding generation is ReLU. We use StepLR as the learning rate scheduler, which decreases by a factor of 0.1 every 5 epochs. The initial embedding vector is generated through Gaussian random initialization. The experiments are conducted on the Intel Xeon Silver 4116 @ 2.10GHz CPU and NVIDIA RTX 2080Ti GPU. The model's parameters are updated through SGD (Stochastic Gradient Descent) and Adam optimizer.

4.3. Evaluation Procedure

We conduct the *top-N* similarity search task to evaluate the model's performance: Given a query trajectory, the model finds N trajectories that are most similar to it.

Assume \mathcal{T} is the set of all trajectories in the dataset, we follow the steps below:

1. For each trajectory $T \in \mathcal{T}$, a specific similarity distance measurement (Fréchet [11] / Hausdorff distance [3]) is used to compute the ground truth distance between T

Methods	Dataset	Backbone	Fréchet			Hausdorff		
			HR@10	HR@50	R10@50	HR@10	HR@50	R10@50
PCA [39]	Porto	Non-learning	0.4203	0.4909	0.8038	0.4850	0.5439	0.8454
SVD [36]		Non-learning	0.4294	0.4977	0.8106	0.4839	0.5436	0.8445
MDS [17]		Non-learning	0.4661	0.5874	0.8607	0.4839	0.6065	0.8770
SRN [27]		RNN+LSTM	0.4720	0.5828	0.7749	0.3800	0.4998	0.7421
NEUTRAJ [42]		RNN+LSTM	0.4801	0.5627	0.8266	0.5025	0.6051	0.8492
node2vec [12]		GNN	0.4175	0.4519	0.7376	0.4317	0.4637	0.7602
VeTraSS (Ours)	GNN	0.4968	0.5853	0.8841	0.5132	0.6275	0.8953	
PCA [39]	Geolife	Non-learning	0.4336	0.5880	0.8446	0.4110	0.5562	0.8243
SVD [36]		Non-learning	0.4438	0.6041	0.8448	0.4081	0.5563	0.8248
MDS [17]		Non-learning	0.4793	0.6187	0.8716	0.3602	0.5472	0.8535
SRN [27]		RNN+LSTM	0.4631	0.6032	0.8121	0.3120	0.4236	0.6640
NEUTRAJ [42]		RNN+LSTM	0.4947	0.6786	0.8403	0.3691	0.4870	0.7416
node2vec [12]		GNN	0.4064	0.4565	0.7268	0.3956	0.4537	0.7461
VeTraSS (Ours)	GNN	0.5003	0.6765	0.8831	0.4862	0.6459	0.8535	

Table 1. **Quantitative comparisons with state-of-the-art models.** VeTraSS outperforms existing state-of-the-art models on the Porto and Geolife datasets under Fréchet and Hausdorff distance. Numbers in **bold**: Highest among all methods. Numbers in blue background: Highest among learning-based methods.

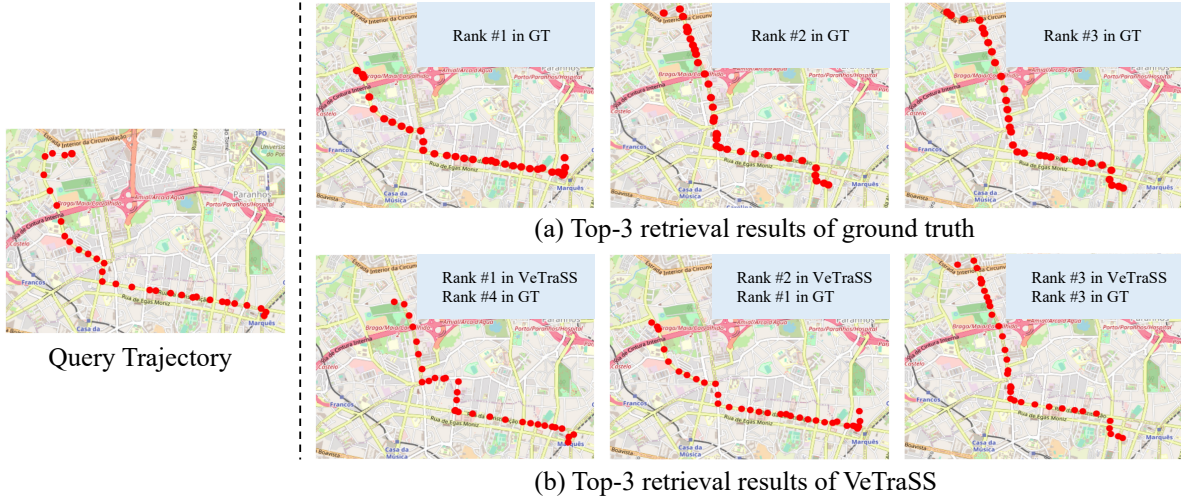


Figure 5. **Qualitative visualization.** **Left**: Query trajectory. The three most similar trajectories are retrieved on the right. **Right (a)**: Top-3 retrieval results of ground truth by computing the real distance as mentioned in Section 4.3. **Right (b)**: Top-3 retrieval results of VeTraSS. It is observed that the retrieval results of VeTraSS closely match the ground truth, qualitatively proving its effectiveness.

and the remaining ones to select its *top-N* similar trajectories. These *N* trajectories from the set Y_T are expressed below:

$$Y_T = \{T_1^G, T_2^G, \dots, T_N^G\}, T_i^G \in \mathcal{T} \quad (16)$$

where G indicates the ground truth domain while Y_T is the *top-N* similar trajectory set for trajectory T specifically.

- For each trajectory T , the model outputs the embedding representation h correspondingly. Therefore, the repre-

sentation of all $T \in \mathcal{T}$ can be expressed as:

$$H = \{h_1, h_2, \dots, h_M\} \quad (17)$$

where M indicates the total number of trajectories.

- For each $h \in H$, the Euclidean distance is computed between h and the remaining ones to form the distance matrix of all representations: $d_{ij} = \|h_i - h_j\|_2$. Therefore, for each trajectory T , the *top-K* similar trajectories set (X_T) based on the above representation distance can

be formed by ranking d_{ij} :

$$X_T = \{T_1^P, T_2^P, \dots, T_K^P\}, T_i^P \in \mathcal{T} \quad (18)$$

where P indicates the model prediction domain while X_T is the $top-K$ similar trajectories from model’s output.

To evaluate the model’s performance, two evaluation metrics are employed:

$$HR@K = \frac{1}{|\mathcal{T}|} \sum_{T \in \mathcal{T}} \frac{|X_T \cap Y_T|}{K}, K = N \quad (19)$$

$$RN@K = \frac{1}{|\mathcal{T}|} \sum_{T \in \mathcal{T}} \frac{|X_T \cap Y_T|}{N}, K \geq N$$

where $HR@K$ refers to the $top-K$ hitting ratio while $RN@K$ indicates the $top-K$ recall for $top-N$ ground truth. Moreover, both two similarity distance measurements (Fréchet / Hausdorff) are applied for comprehensive evaluation.

4.4. Trajectory Similarity Search Performance

We compare VeTraSS’s performance of representation learning with both non-learning-based methods (PCA [39], SVD [36], MDS [17]) and state-of-the-art learning-based ones (SRN [27], NEUTRAJ [42], node2vec [12]).

4.4.1 Quantitative Results

The quantitative results of VeTraSS’s representation learning performance are shown in Table 1. As demonstrated, VeTraSS showcases the effectiveness over existing methods and achieves state-of-the-art performance on Porto and Geolife under two similarity measurement metrics. In Table 1, the results in bold represent the state-of-the-art among all methods (non-learning/learning) while those in the blue background indicate the leading performance among learning-based methods.

In comparison with non-learning methods under Fréchet distance, VeTraSS demonstrates significant improvement over PCA (+7.65%), SVD (+6.74%), and MDS (+3.07%) of HR@10 as an example on Porto. Similar results can be observed under the Hausdorff distance: +2.82% against PCA, +2.93% against SVD and MDS. The remarkable performance on Geolife can also be observed consistently.

In terms of the comparison with existing learning-based models [12, 27, 42], VeTraSS consistently reaches the state-of-the-art under Fréchet / Hausdorff distance. Benefiting from the GNN’s ability to capture global graph-level representations and the adaptability to different graph structures against RNN, a significant improvement can be observed (e.g. +1.67% of HR@10, +2.26% of HR@50, and +5.75% of R10@50 under Fréchet distance on Porto) when compared with NEUTRAJ [42]. Similar observations can

be concluded against SRN [27]. This proves the effectiveness of GNN over RNN as the model backbone in the graph representation learning task. Since node2vec [12] generates representations using general graph-based data (e.g. PPI, Wiki) [12] instead of focusing on trajectory data specifically, it fails to precisely learn the temporal dynamics, coordinates variations, and entity movements, causing a noticeable decrease (7.93% in HR@10, 14.65% in R10@50) in hitting ratio and recall.

4.4.2 Qualitative Results

The qualitative results of VeTraSS (on Porto as an example) are shown in Figure 5, where $top-3$ similar trajectories are retrieved based on the source trajectory on the left. Specifically, the results of ground truth (by computing the actual distance using the Euclidean function in the dataset) and our model are shown. From this figure, it is evidently to conclude that the retrieval results of VeTraSS closely match the ground truth (e.g. Rank #2 in VeTraSS and Rank #1 in ground truth), showcasing the effectiveness of VeTraSS in searching similar trajectories.

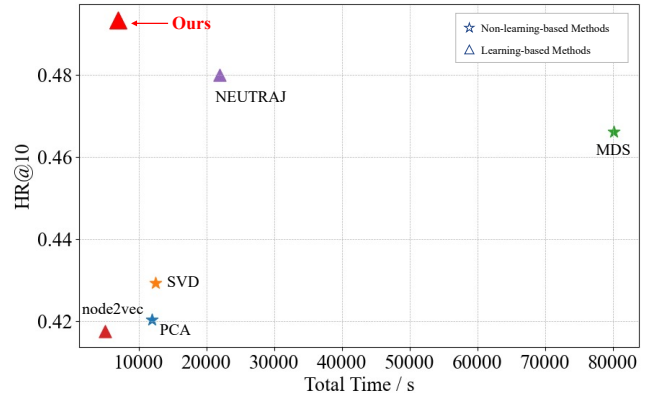


Figure 6. **Efficiency analysis.** The accuracy (HR@10) against the total time for representation learning on Porto is shown, where VeTraSS (ours) represents the highest accuracy of hitting ratio while requiring one of the least time.

4.5. Efficiency Analysis

The model efficiency analysis is shown in Figure 6, including both non-learning and learning-based approaches. Specifically, when compared with the mathematical methods (PCA, SVD, MDS), VeTraSS achieves the highest accuracy (HR@10) while requiring the least time for embedding generation. Moreover, our model outperforms cutting-edge learning-based models significantly. We present substantial advantages in terms of both time cost and performance against NEUTRAJ [42]. In addition, we take approximately the same time cost as node2vec [12] while achieving considerably more accuracy than it does.

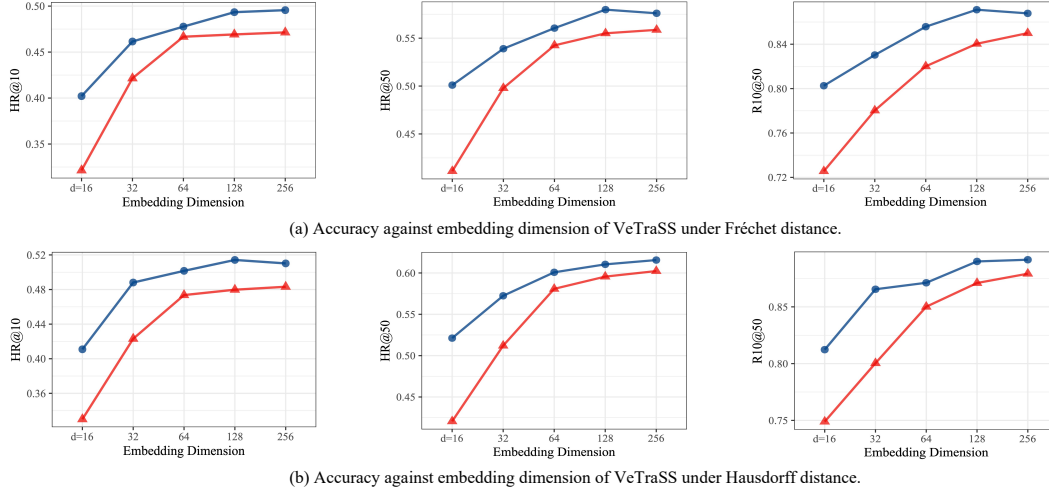


Figure 7. **Ablation studies of VeTraSS on embedding dimension on Porto.** The blue line indicates the final model (VeTraSS with a multi-scale attention module) while the red line represents the single-scale version (VeTraSS_{sing}). **(a):** Accuracy against embedding dimension on Porto under Fréchet distance. **(b):** Accuracy against embedding dimension on Porto under Hausdorff distance.

Methods	Distance	HR@10	HR@50	R10@50
VeTraSS _{sing} w/o SC	Fréchet	0.4692	0.5551	0.8408
		0.4897	0.5710	0.8706
VeTraSS (Ours)		0.4968	0.5853	0.8841
VeTraSS _{sing} w/o SC	Hausdorff	0.4778	0.5956	0.8591
		0.5039	0.5936	0.8752
VeTraSS (Ours)		0.5132	0.6275	0.8953

Table 2. **Ablation study.** This experiment quantitatively shows the effectiveness of the model’s key components on the Porto dataset, including multi-scale design, sequential connection, and embedding dimension.

4.6. Ablation Studies

We conduct a comprehensive analysis of the ablation studies on the model architecture to investigate the impact of key components, including the multi-scale graph attention module, sequential connection (SC), and embedding dimension. The primary goal is to illustrate the model’s performance and the importance of these elements in embedding generation for trajectory similarity search.

Multi-scale Attention Module. From Table 2, a significant drop in all the metrics can be observed when using a single-scale attention structure. Multi-scale attention on multi-scale graphs retains more similarity information and feature associations between nodes (e.g. higher-order neighbors retrieval) than single-scale structure, and these hierarchical features can only be extracted in the higher-scale similarity graphs. Therefore, VeTraSS without such architecture fails to learn deep features for graph representation learning.

Sequential Connection. Hierarchical features and repre-

sentations can be learned through sequential connections to allow the model to learn complex features for graph understanding. As proven in [14, 22], the fusion between multi-scale features will instruct the model to learn deep and superficial levels of abstraction, effectively enhancing the model’s capabilities of graph representation learning.

Embedding Dimension. The ablation studies on the embedding dimension of the representation vectors are shown in Figure 7. When the embedding dimension increases, the performance of the two models (single/multiple attention module) shows a significant increase followed by a stable trend. Increasing the embedding dimension will lead to an improvement in the model’s ability to represent each sample, enabling the representation space to be closer to the original high-dimensional space. Therefore, a large embedding dimension (~ 128) is eventually chosen in the graph representation by VeTraSS.

5. Conclusion

This paper introduces a novel pipeline, VeTraSS, for vehicle trajectory similarity search through graph construction and graph representation learning. VeTraSS first constructs the graph from the original trajectory dataset by generating a distance matrix and applying a threshold determination strategy. Each trajectory is mapped into a node in the graph, while the similarity degree is converted into edge connection weights. Afterward, a novel GNN based on the attention mechanism with multiple layers is designed. The final output as the embedding representation of the original data is concatenated from each layer. Extensive experiments on Porto and Geolife datasets strongly prove the effectiveness of VeTraSS, where our model outperforms existing work

under multiple evaluation metrics and reaches the state-of-the-art. Moreover, we conduct a comprehensive analysis of the ablation studies to investigate the functionality of each key component of the model. Benefiting from the novel design and remarkable performance, VeTraSS showcases its potential to be applied to vehicle trajectory similarity search tasks for autonomous driving in the real world.

References

- [1] Hamidreza Alikhani Koshkak, Ziyu Wang, Anil Kanduri, Pasi Liljeberg, Amir M. Rahmani, and Nikil Dutt. Seal: Sensing efficient active learning on wearables through context-awareness. In *Proceedings of the IEEE/ACM Design, Automation and Test in Europe Conference (DATE'24)*, Spain, 2024. 1
- [2] Faisal Bashir, Wei Qu, Ashfaq Khokhar, and Dan Schonfeld. Hmm-based motion recognition system using segmented pca. In *IEEE International Conference on Image Processing 2005*, pages III–1288. IEEE, 2005. 1
- [3] E Belogay, C Cabrelli, U Molter, and R Shonkwiler. Calculating the hausdorff distance between curves. *Information Processing Letters*, 64(1), 1997. 3, 5
- [4] H Björnsson and SA Venegas. A manual for eof and svd analyses of climatic data. *CCGCR Report*, 97(1):112–134, 1997. 1, 2
- [5] Sarath Chandar, Sungjin Ahn, Hugo Larochelle, Pascal Vincent, Gerald Tesauro, and Yoshua Bengio. Hierarchical memory networks. *arXiv preprint arXiv:1605.07427*, 2016. 2
- [6] Fenxiao Chen, Yun-Cheng Wang, Bin Wang, and C-C Jay Kuo. Graph representation learning: a survey. *APSIPA Transactions on Signal and Information Processing*, 9:e15, 2020. 2
- [7] Ming Cheng, Xingjian Diao, Shitong Cheng, and Wenjun Liu. Saic: Integration of speech anonymization and identity classification. *arXiv preprint arXiv:2312.15190*, 2023. 1
- [8] Xingjian Diao, Ming Cheng, Wayner Barrios, and SouYoung Jin. Ft2tf: First-person statement text-to-talking face generation. *arXiv preprint arXiv:2312.05430*, 2023. 4
- [9] Xingjian Diao, Ming Cheng, and Shitong Cheng. Av-maskenhancer: Enhancing video representations through audio-visual masked autoencoder. In *2023 IEEE 35th International Conference on Tools with Artificial Intelligence (ICTAI)*, pages 354–360. IEEE, 2023.
- [10] Alexey Dosovitskiy, Lucas Beyer, Alexander Kolesnikov, Dirk Weissenborn, Xiaohua Zhai, Thomas Unterthiner, Mostafa Dehghani, Matthias Minderer, Georg Heigold, Sylvain Gelly, et al. An image is worth 16x16 words: Transformers for image recognition at scale. *arXiv preprint arXiv:2010.11929*, 2020. 4
- [11] Maurice Fréchet. Sur quelques points du calcul fonctionnel. 1906. 3, 5
- [12] Aditya Grover and Jure Leskovec. node2vec: Scalable feature learning for networks. In *Proceedings of the 22nd ACM SIGKDD international conference on Knowledge discovery and data mining*, pages 855–864, 2016. 2, 6, 7
- [13] Tianyu Gu, Jarrod Snider, John M Dolan, and Jin-woo Lee. Focused trajectory planning for autonomous on-road driving. In *2013 IEEE Intelligent Vehicles Symposium (IV)*, pages 547–552. IEEE, 2013. 2
- [14] Hanjiang Hu, Zhijian Qiao, Ming Cheng, Zhe Liu, and Hesheng Wang. Dasgil: Domain adaptation for semantic and geometric-aware image-based localization. *IEEE Transactions on Image Processing*, 30:1342–1353, 2020. 1, 8
- [15] Jianying Huang, Jinhui Li, Jeill Oh, and Hoon Kang. Lstm with spatiotemporal attention for iot-based wireless sensor collected hydrological time-series forecasting. *International Journal of Machine Learning and Cybernetics*, pages 1–16, 2023. 2
- [16] Julia Kabalar, Shun-Cheng Wu, Johanna Wald, Keisuke Tateno, Nassir Navab, and Federico Tombari. Towards long-term retrieval-based visual localization in indoor environments with changes. *IEEE Robotics and Automation Letters*, 8(4):1975–1982, 2023. 1
- [17] Joseph B Kruskal and Myron Wish. *Multidimensional scaling*. Number 11. Sage, 1978. 1, 6, 7
- [18] Yonghun Kwon, Woojae Kim, and Inbum Jung. Neural network models for driving control of indoor autonomous vehicles in mobile edge computing. *Sensors*, 23(5):2575, 2023. 1
- [19] Xiucheng Li, Kaiqi Zhao, Gao Cong, Christian S Jensen, and Wei Wei. Deep representation learning for trajectory similarity computation. In *2018 IEEE 34th international conference on data engineering (ICDE)*, pages 617–628. IEEE, 2018. 2
- [20] Yujia Li, Daniel Tarlow, Marc Brockschmidt, and Richard Zemel. Gated graph sequence neural networks. *arXiv preprint arXiv:1511.05493*, 2015. 2
- [21] Wontek Lim, Seongjin Lee, Myoungsoo Sunwoo, and Kichun Jo. Hybrid trajectory planning for autonomous driving in on-road dynamic scenarios. *IEEE Transactions on Intelligent Transportation Systems*, 22(1):341–355, 2019. 2
- [22] Tsung-Yi Lin, Piotr Dollár, Ross Girshick, Kaiming He, Bharath Hariharan, and Serge Belongie. Feature pyramid networks for object detection. In *Proceedings of the IEEE conference on computer vision and pattern recognition*, pages 2117–2125, 2017. 8
- [23] Yixin Liu, Yizhen Zheng, Daokun Zhang, Vincent CS Lee, and Shirui Pan. Beyond smoothing: Unsupervised graph representation learning with edge heterophily discriminating. In *Proceedings of the AAAI conference on artificial intelligence*, pages 4516–4524, 2023. 2
- [24] Zhijun Liu, Chao Huang, Yanwei Yu, Peng Song, Baode Fan, and Junyu Dong. Dynamic representation learning for large-scale attributed networks. In *Proceedings of the 29th ACM International Conference on Information & Knowledge Management*, pages 1005–1014, 2020. 2
- [25] Luís Moreira-Matias, João Gama, Michel Ferreira, João Mendes-Moreira, and Luís Damas. Time-evolving od matrix estimation using high-speed gps data streams. *Expert systems with Applications*, 44:275–288, 2016. 2, 5
- [26] S Narmadha and V Vijayakumar. Spatio-temporal vehicle traffic flow prediction using multivariate cnn and lstm model. *Materials today: proceedings*, 81:826–833, 2023. 1

- [27] Wenjie Pei, David MJ Tax, and Laurens van der Maaten. Modeling time series similarity with siamese recurrent networks. *arXiv preprint arXiv:1603.04713*, 2016. [2](#), [6](#), [7](#)
- [28] Bryan Perozzi, Rami Al-Rfou, and Steven Skiena. Deepwalk: Online learning of social representations. In *Proceedings of the 20th ACM SIGKDD international conference on Knowledge discovery and data mining*, pages 701–710, 2014. [2](#)
- [29] Jiezhong Qiu, Qibin Chen, Yuxiao Dong, Jing Zhang, Hongxia Yang, Ming Ding, Kuansan Wang, and Jie Tang. Gcc: Graph contrastive coding for graph neural network pre-training. In *Proceedings of the 26th ACM SIGKDD international conference on knowledge discovery & data mining*, pages 1150–1160, 2020. [2](#)
- [30] Whitman Richards and Jan J Koenderink. Trajectory mapping: a new nonmetric scaling technique. *Perception*, 24(11):1315–1331, 1995. [1](#)
- [31] Muhammad Shaheer, Jose Andres Millan-Romera, Hriday Bavle, Jose Luis Sanchez-Lopez, Javier Civera, and Holger Voos. Graph-based global robot localization informing situational graphs with architectural graphs. *arXiv preprint arXiv:2303.02076*, 2023. [1](#)
- [32] Sainbayar Sukhbaatar, Jason Weston, Rob Fergus, et al. End-to-end memory networks. *Advances in neural information processing systems*, 28, 2015. [2](#)
- [33] Jian Tang, Meng Qu, Mingzhe Wang, Ming Zhang, Jun Yan, and Qiaozhu Mei. Line: Large-scale information network embedding. In *Proceedings of the 24th international conference on world wide web*, pages 1067–1077, 2015. [2](#)
- [34] Ashish Vaswani, Noam Shazeer, Niki Parmar, Jakob Uszkoreit, Llion Jones, Aidan N Gomez, Łukasz Kaiser, and Illia Polosukhin. Attention is all you need. *Advances in neural information processing systems*, 30, 2017. [4](#)
- [35] Petar Veličković, William Fedus, William L Hamilton, Pietro Liò, Yoshua Bengio, and R Devon Hjelm. Deep graph info-max. *arXiv preprint arXiv:1809.10341*, 2018. [2](#)
- [36] Michael E Wall, Andreas Rechtsteiner, and Luis M Rocha. Singular value decomposition and principal component analysis. In *A practical approach to microarray data analysis*, pages 91–109. Springer, 2003. [6](#), [7](#)
- [37] Ziyu Wang, Nanqing Luo, and Pan Zhou. Guardhealth: Blockchain empowered secure data management and graph convolutional network enabled anomaly detection in smart healthcare. *Journal of Parallel and Distributed Computing*, 142:1–12, 2020. [1](#)
- [38] Ziyu Wang, Zhongqi Yang, Iman Azimi, and Amir M Rahmani. Differential private federated transfer learning for mental health monitoring in everyday settings: A case study on stress detection. *arXiv preprint arXiv:2402.10862*, 2024. [1](#)
- [39] Svante Wold, Kim Esbensen, and Paul Geladi. Principal component analysis. *Chemometrics and intelligent laboratory systems*, 2(1-3):37–52, 1987. [1](#), [2](#), [6](#), [7](#)
- [40] Keyulu Xu, Weihua Hu, Jure Leskovec, and Stefanie Jegelka. How powerful are graph neural networks? *arXiv preprint arXiv:1810.00826*, 2018. [2](#)
- [41] Xinyu Yang, Haoyuan Liu, Ziyu Wang, and Peng Gao. Zebra: Deeply integrating system-level provenance search and tracking for efficient attack investigation. *arXiv preprint arXiv:2211.05403*, 2022. [1](#)
- [42] Di Yao, Gao Cong, Chao Zhang, and Jingping Bi. Computing trajectory similarity in linear time: A generic seed-guided neural metric learning approach. In *2019 IEEE 35th international conference on data engineering (ICDE)*, pages 1358–1369. IEEE, 2019. [2](#), [3](#), [5](#), [6](#), [7](#)
- [43] Yuanfan Yao, Ziyu Wang, and Pan Zhou. Privacy-preserving and energy efficient task offloading for collaborative mobile computing in iot: An admm approach. *Computers & Security*, 96:101886, 2020. [1](#)
- [44] Hanyuan Zhang, Xingyu Zhang, Qize Jiang, Baihua Zheng, Zhenbang Sun, Weiwei Sun, and Changhu Wang. Trajectory similarity learning with auxiliary supervision and optimal matching. 2020. [2](#)
- [45] Lu Zhang, Weiqi Feng, Chao Li, Xiaofeng Hou, Pengyu Wang, Jing Wang, and Minyi Guo. Tapping into nfv environment for opportunistic serverless edge function deployment. *IEEE Transactions on Computers*, 71(10):2698–2704, 2021. [1](#)
- [46] Lu Zhang, Chao Li, Xinkai Wang, Weiqi Feng, Zheng Yu, Quan Chen, Jingwen Leng, Minyi Guo, Pu Yang, and Shang Yue. First: Exploiting the multi-dimensional attributes of functions for power-aware serverless computing. In *2023 IEEE International Parallel and Distributed Processing Symposium (IPDPS)*, pages 864–874. IEEE, 2023. [1](#)
- [47] Yifan Zhang, An Liu, Guanfeng Liu, Zhixu Li, and Qing Li. Deep representation learning of activity trajectory similarity computation. In *2019 IEEE International Conference on Web Services (ICWS)*, pages 312–319. IEEE, 2019. [2](#)
- [48] Yu Zheng, Xing Xie, Wei-Ying Ma, et al. Geolife: A collaborative social networking service among user, location and trajectory. *IEEE Data Eng. Bull.*, 33(2):32–39, 2010. [2](#), [5](#)
- [49] Silin Zhou, Jing Li, Hao Wang, Shuo Shang, and Peng Han. Grlstm: trajectory similarity computation with graph-based residual lstm. In *Proceedings of the AAAI Conference on Artificial Intelligence*, pages 4972–4980, 2023. [2](#)
- [50] Ziyi Zhou, Baoshen Guo, and Cao Zhang. Doseguide: A graph-based dynamic time-aware prediction system for post-operative pain. In *2021 IEEE 27th International Conference on Parallel and Distributed Systems (ICPADS)*, pages 474–481. IEEE, 2021. [1](#)